




Efficiency of combined MA-XRF and CXRF to give nondestructive insights about changes of a historical painting

José Tapia¹, Myriam Eveno^{1,2}, Thomas Calligaro^{1,2,3}, Laurent Pichon^{2,3}, Eric Laval², Elisabeth Ravaud^{1,2}, Ina Reiche^{1,3,a} 

¹ Chimie ParisTech-CNRS, IRCP, UMR8247, PSL Research University, 75005 Paris, France

² Centre de recherche et de restauration des musées de France, C2RMF, 75001 Paris, France

³ Fédération de Recherche FR3506 CNRS New AGLAE, Centre de recherche et de restauration des musées de France (C2RMF), 75001 Paris, France

Received: 30 September 2022 / Accepted: 13 December 2022

© The Author(s) 2023

Abstract Historical paintings with important iconographical changes represent an analytical challenge. Considering the case study of a fifteenth-century French painting studied during its restoration, the efficiency of a combined noninvasive approach of two-dimensional scanning macro-X-ray fluorescence imaging (MA-XRF) and a laboratory-based depth-resolved confocal micro-X-ray fluorescence (CXRF) is discussed. Large chemical maps of several elements were obtained by MA-XRF, enabling the identification of zones of interest representing changes in the painting composition. In these areas, depth profiles were measured with CXRF, allowing to evidence overlaying paint layers. The advantages of this technique are that it can give direct information on the stratigraphy of paint layers in a nondestructive way and can reduce the sampling needed, as well as increase the locations analyzed (in our study twenty-two depth-resolved scans). These results complement information obtained by scanning electron microscopy coupled with an energy-dispersive X-ray analyzing system (SEM–EDX) on three cross-sectional samples taken in the areas of interest. Additionally, the three cross sections of the painting were studied by CXRF lateral scans (y) in order to evaluate the efficiency of the CXRF analyses against SEM–EDX. The study shows the benefits of the combination of MA-XRF and CXRF for analyzing painting compositions, as such a high number of cross sections would have been impossible to sample. From an art-historical and conservation perspective, this combined study provides an understanding of the original painting's paint sequence and its later retouches, helping to make informed conservation treatment decisions.

1 Introduction

X-ray fluorescence (XRF) is an efficient, fast, noninvasive, safe and firmly established method for measuring single spots on artworks and obtaining information on the elemental composition [1], using an X-ray beam of small diameter and a detector [2, 3]. An evolution of this method is the two-dimensional (2D) scanning macro-X-ray fluorescence spectroscopy imaging (MA-XRF), that allows recording spectra point by point along the work area [3], providing relatively large elemental maps of the painting down to trace concentrations (sometimes up to several square meters [4]). Moving the painting with a motorized X–Y stage [5], a scan can be done in just hours, sometimes a few days for big paintings. It is a well-established method that can use both synchrotron radiation and laboratory X-ray generators [4, 5]. However, MA-XRF presents limitations [2] like the fact that the resolution is limited by the size of the X-ray beam or moreover, that the stratigraphy of the paintings cannot be directly resolved, which can be a major issue when investigating the painting's technique and the changes it might have undergone.

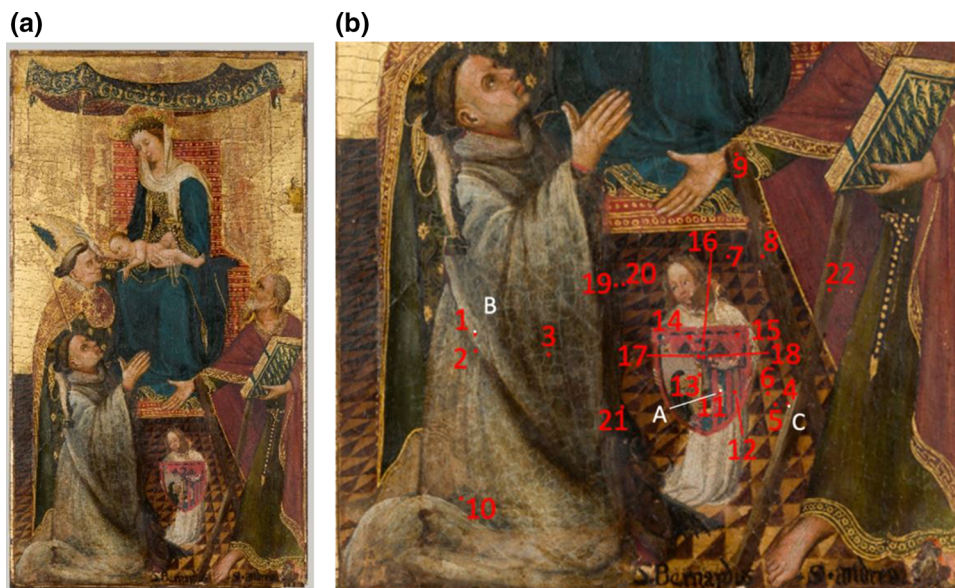
The analysis of the stratigraphy of paintings is traditionally performed by means of optical microscopy and electron microscopy coupled with an energy-dispersive X-ray system (OM and SEM–EDX) on cross sections [6]. However, these analyses require micro-sampling, in most cases a not acceptable process [1].

To solve this last problem, a laboratory-based noninvasive depth-resolved confocal micro-X-ray fluorescence (CXRF) spectrometer called LouX^{3D} was developed at the C2RMF laboratory a few years ago [3, 6, 7]. By using a confocal system consisting of two X-ray optics, one in the excitation channel and the other in front of the detector, an ellipsoidal micro-volume can be defined by the overlap of the foci of both optics [7], the size of it depending on the X-ray energy [6]. First proposed by Gibson and Kumakhov in the 1990s [8], this method allows to visualize the stratigraphy of the layers with a nondestructive approach. The first applications of such device used synchrotron radiation [1, 9, 10], but it can now be found in several laboratories due to the existence of relatively

Focus Point on Scientific Research in Cultural Heritage 2022 Guest editors: L. Bellot-Gurlet, D. Bersani, A.-S. Le Hô, D. Neff, L. Robinet, A. Tournié.

^a e-mail: ina.reiche@chimieparitech.psl.eu (corresponding author)

Fig. 1 **a** Photograph of the painting “Virgin and Child surrounded by saints and a donor” (RFML.PE.2018.51.1). © C2RMF, T. Clot and **b** detail showing the locations where the three cross sections were taken in white (A, B and C), and in red the 22 locations where CXRF depth profiles were performed



small X-ray generators [1, 7, 9–20]. This analysis allows for the exploration of the paint layer construction, its chemistry and its stratigraphy, as complex layers and overpaints can be identified in depth-resolved scans. Thus, it is a promising analytical technique allowing for the nondestructive investigation of objects with a layered structure.

In this work the efficiency of CXRF is evaluated for the study of complex painting stratigraphy with respect to MA-XRF and SEM–EDX on cross sections. A painting was studied, allowing to address the challenging questions arising from the multiple changes it had undergone through time, using a combination of CXRF and MA-XRF analysis, while at the same time confirming that the CXRF measurements are right.

The goal of this study is to establish and characterize the original materials, the later additions and the paint palette used by the painter, helping in the decision-making process of the restoration. This complimentary approach therefore allowed revealing information about former compositions and provided insights into the genesis of the painting, unraveling the secrets hidden deep within the layers.

2 Experimental section

2.1 Materials

The painting *Virgin and Child surrounded by saints and a donor* (anonymous, France, inv. no. RFML.PE.2018.51.1, Fig. 1a and b) is considered to have been composed in France between 1420 and 1430 and is conserved in the Louvre Museum. It consists of a single oak panel, with a size of $23.7 \times 42.5 \text{ cm}^2$. It has been studied during the restoration process. Three cross sections were also taken at the C2RMF laboratory (A: no. 20041, B: no. 20042 and C: no. 20043), one of each of the three areas of interest found with the MA-XRF mapping, to be analyzed by SEM–EDX. This analysis, the lateral scan (y) on the cross sections, and the three depth-resolved scans (z) in points adjacent to where the micro-samples had been taken from, allowed to compare between the SEM–EDX and CXRF results. After confirming that CXRF was indeed a correct alternative allowing to distinguish the layers and elements seen by SEM–EDX (when heavier than Si), nineteen other depth-resolved scans were performed in the three areas of interest. This technique thus changes the analytical conditions and makes time, and not the permission to take micro-samples, the limit of the study.

2.2 Methods

2.2.1 Scanning macro-X-ray fluorescence (MA-XRF)

The detailed description of the instrument used in this study can be found in [2, 21]. It consists of a head mounted on a motorized X–Y stage allowing for movement along the artwork (X max 50 cm, Y max 60 cm, ZABER). The 15 kg head comprises an X-ray generator (ROENTEC X1 generator, Mo tube model RTW MCB 50–0.6, 50 kV, 0.6 mA max), a fast silicon drift X-ray spectrometer collecting the XRF data (Amptek model X123, 70 mm^2 active area collimated to $50 \mu\text{m}^2$ Fast SDD), and a laser allowing precise alignment working in concordance with a micro-video camera (Toshiba QP49H, 8 mm objective). A 0.6-mm diameter Mo pinhole

Fig. 2 CXRF prototype LouX^{3D} used with the painting at the C2RMF laboratory, Paris



collimator is situated at the X-ray source end to shed a parallel and wide energy range beam (1.8–40 keV) on the painting. The detector was placed at a distance of 15 mm from the paintings' surface. In our case, three maps of 490×870 , 340×420 and 250×250 pixels were acquired (whole painting, plus two details in the donor's tunic and the coat of arms) corresponding to sizes of (x,y) 24.5×42.5 , 17×21 and 5×5 cm² area. At max size, a scanning speed of 12.5 mm/s and a dwell time of 40 ms were used, taking 4.7 h to collect the whole elemental maps. The two small scans were performed in areas selected according to the most interesting zones identified in the first scan. A dedicated program implemented in a portable computer running Windows ® using a Visual studio-built interface controls the instrument [2]. Spectra are collected on the fly, and normalized to a common live time just after the transfer.

Data evaluation The data (a matrix of pixels each containing a spectrum) are stored in EDF format, and processed with the open source program PyMCA [5, 22], developed for X-ray fluorescence at the European Synchrotron Facility (ESRF). With it, we can fit the peak area of different elements (in our study, namely Ca, Mn, Fe, Cu, Zn, As, Ba, Au, Hg and Pb), and obtain elemental maps in PNG format. These maps can then be represented in a linear or logarithmic black- and white-contrast scale in order to enhance the visibility (a higher value of white indicates a stronger signal). For all images, minimum and maximum intensity values were selected to enhance the readability.

2.2.2 Optical microscopy, and scanning electron microscopy coupled with an energy-dispersive X-ray analyzing system (SEM–EDX)

The three cross sections were investigated by optical microscopy (OM; Nikon Eclipse LV-100ND coupled with a Nikon DS-Ri1 camera) under visible and UV lights. They were later analyzed using a scanning electron microscope (SEM; Philips XL30 CP: tungsten cathode, backscattered electron detector) coupled with energy-dispersive X-ray spectroscopy (EDX; Oxford Instruments, AZtec software) using an accelerating voltage of 20 kV. The samples were polished and carbon-coated to avoid surface charging.

2.2.3 Confocal micro-X-ray fluorescence (CXRF) prototype LouX^{3D}

Confocal micro-X-ray fluorescence was performed on the painting using the LouX^{3D} spectrometer [7] installed at the C2RMF laboratory in Paris (Fig. 2). By moving the artwork through the probing volume with micrometer accuracy, a depth scan can be performed, allowing the elemental distributions inside the sample to be explored. In this device, the object is placed on a motorized X–Y–Z stage, and moved away from the measurement head for security reasons. The device specifications can be found with more detail in [7]. The X-ray tube is an Rh anode (IMOXS), operated at 50 kV and 0.6 mA max, equipped with a full polycapillary lens at the exit providing a spot size of 50 μm and a working distance of about 6 mm. On the detection channel, an X-Flash detector (Bruker AXS, Rontec X Flash series 4 model 4010) is used with a poly-Conical Capillary Collimator (CCC) lens set up in front of it with a focal distance of 11 mm. The energy range of the systems is limited by the transmission of the optics between 3 and 20 keV. In previous studies [6, 7], paint layers up to 15–20 μm could be identified with the LouX^{3D} device by elemental profiling in the lateral direction on a painting's cross section.

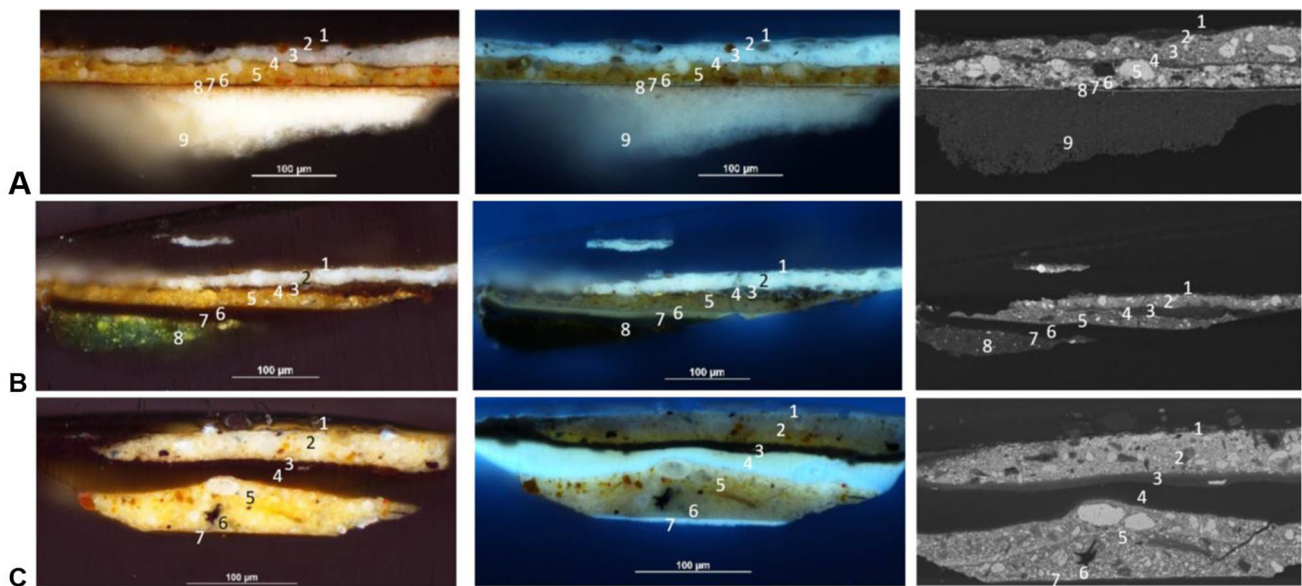


Fig. 3 Optical (left), UV (center) and backscattered electron micrographs (right) of cross sections **A**, **B** and **C** with the different layers numbered

On the three cross sections, lateral CXRF scans (y) were applied to allow a comparison with optical microscopy (OM) and SEM–EDX measurements. For each lateral position (y), the acquisition time per spectrum was 100 s, with a step between measurements of 10 μm .

Nevertheless, depth scans (z) were taken at different locations for the most part. The acquisition time per spectrum at each analysis depth was also set to 100 s. However, from the measurement of depth profiles, at greater depths an attenuation effect can be observed due to the attenuation and absorption of the X-rays by the surrounding and top layers. If heavy elements like Pb or Hg are on the outer layers of the painting, they will absorb even more the X-ray emission of elements of deep layers, thus getting less intensity and precluding the measurement of these deeper layers. Indeed, deeply buried layers often cannot be detected due to this absorption effects. If no heavy elements are present on the surface layers, a depth of 100–150 μm can be reached in paintings. Because of this, the time of acquisition of a complete depth scan generally takes 35 (when many heavy elements are present on the surface) to 60 min.

Depth scans were first performed in the vicinity of the three cross-sectional sampling locations, to be extended to other locations in the areas of interest. For each depth scan, the object was placed on the motorized sample stage, positioned with the aid of the device’s optical microscope, and subsequently submitted to two scans. The first one, a fast scan with a step of 50 μm , was mainly to locate the values of z where signal was measured. The second, a precise scan with a step of 10 μm was performed in the interval of interest by moving the painting away of the instrument starting at the deepest detectable layer, and measuring a spectrum per value of z .

Data evaluation The XRF spectra obtained for each depth value were fitted by means of the PyMCA program [22]. The peak areas of the different elements were adjusted, and the net peak intensities of the characteristic fluorescence lines were extracted and normalized to their maxima. These normalized values were then plotted against the depth z value, enabling an easier comparison of the intensity vs depth profiles. As in the MA-XRF case, the elements mainly found were Ca Mn, Fe, Cu, Zn, As, Ba, Au, Hg and Pb. The maximum intensities of the element peaks indicate the location of the different layers. These layers are labeled starting from the surface. This way is unconventional in the description of paint layer succession (usually starting at the bottom) but is justified here because the deeper layers can often not be detected due to absorption effects by CXRF. It has to be noted that the distances depicted in the CXRF depth profiles do not correspond to real thicknesses of paint layers.

3 Results and discussion

3.1 Characterization of the CXRF scan performances with respect to the study of the paint stratigraphy

The analytical volume was characterized with thin metallic films prior to the measurements presented in the following paragraph. For this, several films of 1 μm of thickness were scanned in depth with a step size of 10 μm . Several elements were used (Cr, Fe, Ni, Cu, Zn, and Pb). We measured the full width at half maximum (FWHM) of each depth profile obtained representing the intensity of

the peak of the different elements vs the position z . As expected, we obtained a FWHM decreasing with increasing energy: 61 μm at 6.4 keV and 36 μm at 12.6 keV for example.

Three samples for the cross sections A, B and C were taken on the painting and their position is shown in Fig. 1b. They were first analyzed with optical microscopy (OM) and then by SEM–EDX. Figure 3 shows the cross sections under visible and UV light, as well as their corresponding backscattered electron micrographs. These techniques allow us to view the limits but also the advantages and precision of the CXRF setup. In Table 1 a detailed description of the layers in each cross section obtained by OM and SEM–EDX observations can be found, enriched with the comparison with the CXRF lateral scan (y) of the cross sections. The results from the CXRF depth scans (z) of the locations adjacent to the sampling are also presented. It can be recognized how the CXRF lateral scan (y) of cross section A allows identifying four out of the nine (4/9) layers determined by OM/SEM–EDX, 4/8 for B, and 4/7 for C. In the case of the CXRF depth scans of the locations adjacent, we have 2/6 for A, 5/8 for B, and 3/7 for C. This allows us to perform another comparison between what can be detected by CXRF regarding a typical analysis on cross sections by OM and SEM–EDX. The high proportion of layers detected by the lateral and depth CXRF scans is not a phenomenon unique to this artwork but is also shared with other paintings analyzed with the Loux^{3D} setup going from those of Italian Renaissance artists to nineteenth-century French painters (Table A in the supplementary information, SI).

In Fig. 4a is presented the CXRF sum spectrum for the depth scan (z) at the analysis point 1, adjacent to where the cross section B was taken. This spectrum reveals the presence of Pb, Fe, Mn, Cu, Au, Hg and Ca at this position. The CXRF lateral profile (y) in the cross section B shows the layers described in Table 1. Indeed, we first see on the surface a layer with two peaks, Pb and Fe, followed by an Au layer (Fig. 4b), and then very well separated, a Cu-based layer. Almost the same results are found when performing a depth profile at the analysis location 1 adjacent to where the sample had been preserved (Fig. 4c).

As can be seen, CXRF resolves quite well the different layers. By using CXRF the number of cross sections collected in an artwork can be limited. Only one sample is needed to verify that the gap between layers is a varnish, and many more CXRF depth scans can be performed without the need to do more sampling. The varnish was also observed using Fourier-transform infrared spectroscopy (FTIR) on some cross sections (Fig. I in SI).

3.2 Chemical imaging for inferring characteristic pigments in the paint layers of the figurative depictions

A MA-XRF mapping of the whole painting was performed. Several areas of interest were identified: the coat of arms and the monk's tunic where several successive interventions were highlighted, and the cross. Indeed, on top of the original coat of arms had been applied two others, but it was difficult to understand the order and their shape as MA-XRF gives limited depth-resolved information. On top of the donor's short tunic had been applied a longer one, changing the iconography of the painting by turning him into a monk character. The cross could be original, but could have also been added at the same time as the iconographic change.

Figure 5a shows the sum MA-XRF spectrum produced by a $17 \times 21 \text{ cm}^2$ area (340×420 pixels), presenting a detail of the whole painting including the monk's tunic, the coat of arms, and a part of the cross. The chemical maps of significant elements are shown in Fig. 5 b–f. A linear scale is applied here except in the case of lead and gold where a logarithmic greyscale is applied to compensate for the differences in recorded intensities. Comparing the Pb and Cu maps (Fig. 5b and c, respectively), we can see how they look very different in the monk's tunic, the coat of arms, and the cross. The Cu map shows a short tunic and the donor's legs, and a coat of arms composed of crescent moons of a different element surrounded by a Cu-based pigment. The cross does not seem to appear, even though some parts can be deduced from the missing intensity of the Cu triangles that has been absorbed by other elements. However, looking at the Pb map the composition seen is different: the tunic is long, the coat of arms is a rooster on a column, and the cross appears clearly. Furthermore, the Hg map (Fig. 5d) reveals a third different coat of arms conformed by a red pigment rectangle above spaced red stripes. Also, details appear on the tunic collar and cuffs that can only belong to the original underlying tunic, as the visible one is white and brown with no red. The Fe map (Fig. 5e) reinforces the existence of a shorter tunic, which then has to be blue/green with brown, and shows the same coat of arms as the lead map. The cross is perfectly visible, showing the colors we see, brown with white. The Au map (Fig. 5f) provides some golden details on the bishop's dress that are hidden in the visible composition, strengthening our knowledge on what is behind the long monk's tunic. Furthermore, details in the tunic collar and cuffs give us information in addition to the Hg map that these might be red vermilion with some golden touches. The MA-XRF clearly shows here its ability to evidence distinct paint areas in a nondestructive way, even though it is lacking the ability to give depth-resolved information.

3.3 Depth profiling for elucidating the painting's stratigraphy and new information obtained on the three areas of interest

Twenty-two CXRF depth profiles (z) were performed on the painting (Fig. IIa–n in SI). The locations are marked in Fig. 1b in a detail of the painting at a moment prior to the analysis, when the restoration had already begun. The depth profiles taken at six representative locations are presented in Fig. 6a–f and discussed in this section, as well as the previously presented location 1 (Fig. 4c). They comprise the three main areas of interest detected in the MA-XRF elemental maps: the monk's tunic, the coat of arms, and the cross. Location 1, 3 and 10 are located in the monk's tunic, location 11 and 12 in the coat of arms, and 8 and 22 in the cross.

Table 1 OM and SEM-EDX descriptions of the paint layers compared with CXRF lateral scans (y) of the cross sections and CXRF depth scans (z) of adjacent points.

Cross section	Layer and composition determined by OM/ SEM-EDX observations	Elements identified by CXRF lateral scan (y)	Elements identified by CXRF depth scans (z) of adjacent locations	Identification
A	<i>Location 11</i>			
	1. Thin fluorescent under UV layer (several μm)			
	2. Thin organic layer with big orange grains (red ochre; Al, Si, Fe) (several μm)	(Fe) right next to <u>Cu</u>		Coat of arms 3
	3. Light beige layer (lead white; Pb, Ca) with small red, black and blue grains (Cu) as well as grains of green earth (10–30 μm)	<u>Cu</u>		
	4. Organic layer, possible varnish (several μm)			Coat of arms 2
	5. Beige-orange layer of lead white (Pb, Fe, Ca) with red, white and black grains (earth pigments, vermilion; Ca, Fe, Hg, S, Mg) (15–25 μm)	Fe, <u>Hg</u> , <u>Pb</u>	Fe, <u>Hg</u> , <u>Pb</u>	
	6. Organic layer, possible varnish (several μm)			Coat of arms 1
	7. Gold leaf (Au)	<u>Au</u>	<u>Au</u>	
	8. Bole (earth pigments; Al, Si, Mg, Fe) (several μm)	Not clear. <u>Fe</u> , <u>Hg</u>		
	9. White ground layer (calcium carbonate with several alumina silicates; Ca, Al, Si) (66 μm)			
B	<i>Location 1</i>			
	1. Organic layer with orange and yellow grains (Pb, Ca). Possibly tinted varnish (several μm)		(Fe), <u>Pb</u>	Monk's tunic
	2. Lead white and earth pigments (Mg, Al, Si, Fe) with a P, Cl, Pb and Ca layer on the surface (13–16 μm)	Fe, <u>Pb</u>	Fe, <u>Pb</u>	Monk's tunic
	3. Brown organic non-fluorescent under UV layer with some earth elements (Al, Si) (13 μm)			Golden detail
	4. Gold leaf (Au)	<u>Au</u>	<u>Au</u>	Golden detail
	5. Beige mordant layer (lead white, earth pigments, lead tin yellow; Pb, Sn, Al, Si, Fe) (13–17 μm)	Not clear	Not identified	Golden detail
	6. Organic layer, possibly varnish (~7 μm)			Bishop's green tunic
	7. Copper green glaze non-UV-fluorescent layer (Cu, Pb, Sn) (5–6 μm)	Cu	<u>Cu</u> , <u>Pb</u>	Bishop's green tunic
	8. Green copper layer with some grains of lead tin yellow (Cl, Sn and Pb) (30 μm)	<u>Cu</u>	<u>Cu</u> , <u>Pb</u>	Bishop's green tunic
	No ground layer present in this cross section			

Table 1 continued

Cross section	Layer and composition determined by OM/ SEM-EDX observations	Elements identified by CXRF lateral scan (y)	Elements identified by CXRF depth scans (z) of adjacent locations	Identification
C	<i>Location 4</i>			
	1. Slightly fluorescent under UV organic layer, perhaps a tinted varnish (several μm)	<u>Fe</u> , <u>Pb</u>	<u>Fe</u> , <u>Hg</u>	Cross
	2. Light beige layer with lead white, earth pigments, blue copper pigment, orange iron oxide and carbon black (20–25 μm)	(<u>Fe</u>), <u>Cu</u> , <u>Pb</u>	<u>Pb</u>	Cross
	3. Thick non-fluorescent under UV organic layer with some Cu and Pb (5–6 μm)	Not clear	Not clear	Triangle
	4. Thick organic varnish layer fluorescent under UV (8–20 μm)			Floor
	5. Beige layer (lead white, orange iron oxide, vermilion) (13–16 μm)	<u>Fe</u> , <u>Hg</u> , <u>Pb</u>	<u>Cu</u> , <u>Hg</u> , <u>Pb</u>	Floor
	6. Beige layer (lead white, earth pigments; Al, Si, Fe) (15–25 μm)	<u>Pb</u>	Not identified	Floor
	7. Thin organic layer of impregnation (several μm)			
	No ground layer present in this cross section			

Layer one represents the outer layer closest to the surface of the painting. The element underlined (e.g., Cu) means it is the main identifiable element, without underline (e.g., Cu) that it is present, and between parenthesis, e.g., "(Cu)", that it is a minor element. Coat of arms 3 was removed by the restorers between the cross-sectional sampling and the CXRF depth scan

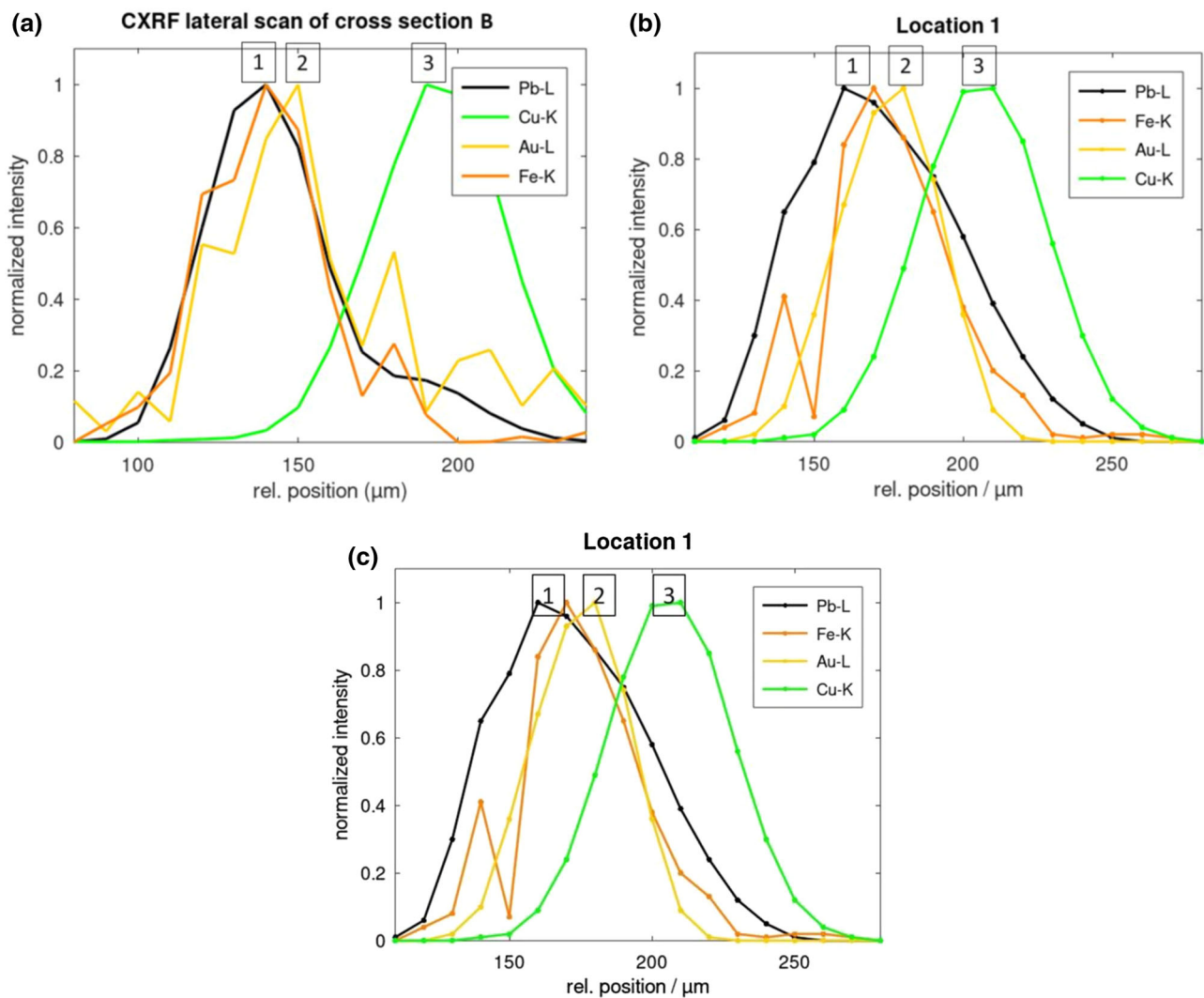


Fig. 4 CXRF results. The left side of the depth and lateral scan profiles represents the painting surface. The identified paint layers are indicated with the numbers on the depth profiles. **a** Sum spectrum of the 36 XRF spectra (one per depth position (z) measured) for the depth scan at analysis Location 1, adjacent to the sample location for the cross section B. Normalized elemental profiles for: **b** lateral scan of cross section B (the intensity maxima of the Fe $K\alpha$, Cu $K\alpha$, Au $L\alpha$ and Pb $L\alpha$ fluorescence lines are 46, 1339, 128 and 18,601, respectively) **c** depth scan for analysis location 1 (adjacent to the sampling of cross section B) (the intensity maxima of the Fe $K\alpha$, Cu $K\alpha$, Au $L\alpha$ and Pb $L\alpha$ fluorescence lines are 376, 9402, 2024 and 11,008, respectively)

The combination of the results obtained by MA-XRF and CXRF, as well as the information provided by SEM–EDX analysis of the cross sections, allows getting new insights into the different repaints and iconographic changes of the painting.

Monk's tunic The profiles for the depth-scans analysis location 1, 3 and 10 correspond to this area. The CXRF depth profile at the analysis location 1 (Fig. 4c) indicates three main paint layers. At the surface of the painting, a Pb- and Fe-based layer containing lead white and earth pigments is identified, corresponding to the long white visible tunic. Below this layer, an Au-based one appears, attributed to a golden detail in the bishop's green cape hidden under the visible white monk's tunic. Under it, and clearly separated from the other layers, is a Cu-based layer that can be attributed to the bishop's green cape.

Figure 6a shows the element depth profiles obtained at analysis location 3 (over the original donor's dress). Two layers can be clearly separated. On the surface, a Pb-based layer with Fe and Ca (lead white and earth pigments) can be correlated to the white monk's tunic. The second one, deeper, is a Cu-based layer containing some Pb. It can be attributed to the short tunic, which should be blue or green (azurite or copper green).

Figure 6b shows the depth profiles at the analysis location 10, in a place of the tunic where the MA-XRF elemental map of Cu shows the feet of the donor. Three layers are identified here. First, a light Ca-based layer is identified on the surface that could indicate the presence of a slightly pigmented varnish. Underneath is found a Pb- and Fe-based layer also containing Ca (lead white with earth pigments), certainly corresponding to the white and brown monk's dress. Finally, at the furthest accessible probing volume is a Cu-based layer, which can be attributed to the feet/pants of the donor, as a little Hg (vermillion, not represented in the graph) content as well as some Fe are also found here.

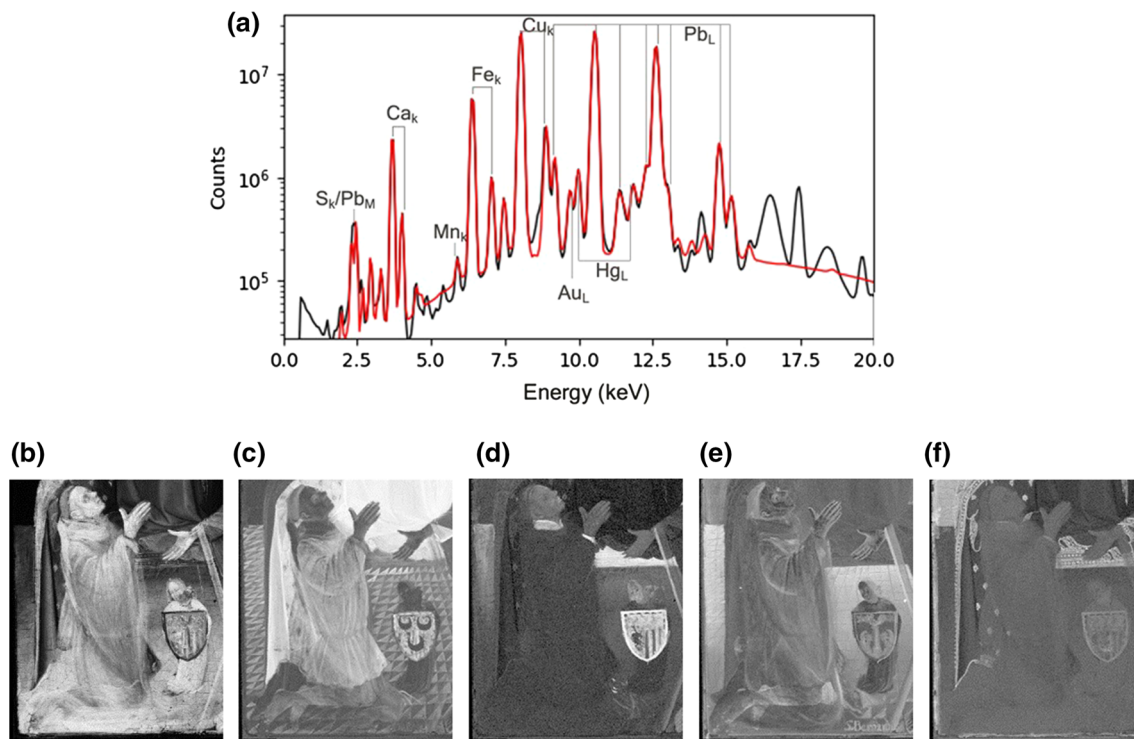


Fig. 5 MA-XRF elemental distribution maps of an area measuring $17 \times 21 \text{ cm}^2$. **a** Experimental sum of the XRF spectra produced by that area together with the fitted spectrum (red line) **b** Pb L in logarithmic scale **c** Cu K **d** Hg L **e** Fe K **f** Au L in logarithmic scale

A shorter tunic under the monk's long white and brown exists (MA-XRF elemental maps of Cu, Fe, Hg and Au). Its color should be dark blue-green, composed of a Cu-based pigment with vermillion and earth pigments at the collar and cuffs. The left side of the long tunic was painted on top of the bishop's Cu-based dress corresponding to a copper green glaze with some lead tin yellow, hiding as well some golden details of it. The CXRF depth scans (locations 1, 2, 3, 10, 19, 20 and 21) find a good separation between the deeper layers (the Cu-based layers of the bishop's dress and the golden detail, the Cu-based layer of the tunic, the floor triangles) and the surface layer (the white tunic). This clear and somewhat big separation was shown to be due to a varnish thanks to the cross section B sampled adjacent to CXRF location 1. This overpaint is important because it changes the iconography of the painting, as the donor was converted into a monk.

Coat of arms The profiles for the depths-scans at analysis location 11 and 12 correspond to the coat of arms. It must be noted here that the painting was analyzed during its restoration, and thus between the moment the MA-XRF elemental maps and cross sections were taken and the moment the CXRF depth profile analysis was performed, some changes had already been undertaken to the painting. Mainly, the third coat of arms on the surface, a cock over a column, had already been partially removed, leaving place to analyze the second and first coat of arms.

The depth profiles at the analysis location 12 (on a beige vertical line in the second coat of arms) are shown in Fig. 6c. Two layers can be resolved very well by looking at the plot. The first one is a layer containing Pb (lead white), Hg (vermillion), Fe (earth pigments) and Ca (possibly calcium carbonate) and is well separated from the second one composed of Cu (likely azurite, as a blue underlayer appears through some small holes). They correspond, respectively, to the second and first coat of arms. We can see the predominance of red pigments in the first layer by looking at the values of the intensity maxima of the Fe K α and Hg L α fluorescence lines.

The CXRF depth scan at the analysis location 11 (on a vertical stripe in the second coat of arms over the gold in the first coat of arms) indicates again two different layers (Fig. 6d). Near the surface, a layer containing Pb, Hg, Fe and some Ca and Cu is found (again, the second coat of arms, lead white, vermillion and earth pigments). Very well separated appears a layer of Au, corresponding to the first coat of arms.

The coat of arms consists in fact of three, painted one over the other. The first coat of arms and deepest is conformed of three golden crescent moons surrounded by a Cu-based pigment, probably azurite. The second is a dragon-shaped figure (location 18 in SI) on a red rectangle (mainly vermillion) in the upper part and alternating beige and red stripes in the lower part. The dragon-figure is made of earth pigments, vermillion and lead white, and perhaps red lake (not detectable by XRF analysis but visible to the observation under the microscope). The third most on the surface is a cock standing on a white column. The Cu MA-XRF elemental map gave information about the first coat of arms, Hg about the second, and Pb and Fe about the third. The Au map gave some insight about the crescent moons, but as the representative peaks of Au and Hg are very close, and the absorption effect at that depth

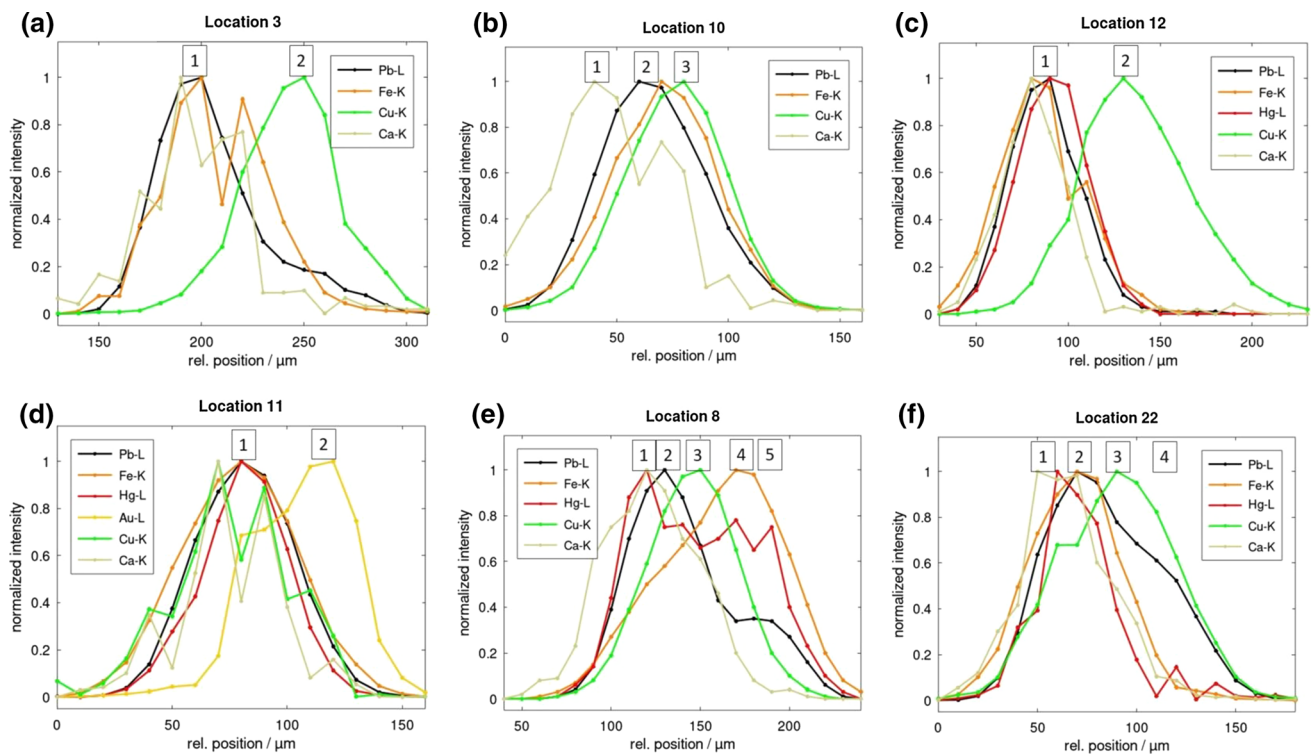


Fig. 6 Results of the CXRF normalized elemental depth profiling. The identified paint layers are indicated with numbers on the depth profiles. **a** Analysis location 3 (the intensity maxima of the Ca $K\alpha$, Fe $K\alpha$, Cu $K\alpha$ and Pb $L\alpha$ fluorescence lines are 19, 1541, 3837 and 22,068, respectively) **b** analysis location 10 (the intensity maxima of the Ca $K\alpha$, Fe $K\alpha$, Cu $K\alpha$ and Pb $L\alpha$ fluorescence lines are 27, 3002, 3294 and 17,546, respectively) **c** analysis location 12 (the intensity maxima of the Ca $K\alpha$, Fe $K\alpha$, Cu $K\alpha$, Hg $L\alpha$ and Pb $L\alpha$ fluorescence lines are 16, 1453, 4298, 1963 and 29,535, respectively) **d** analysis location 11 (the intensity maxima of the Ca $K\alpha$, Fe $K\alpha$, Cu $K\alpha$, Au $L\alpha$, Hg $L\alpha$ and Pb $L\alpha$ fluorescence lines are 18, 1542, 42, 266, 2234 and 23,805, respectively) **e** analysis location 8 (the intensity maxima of the Ca $K\alpha$, Fe $K\alpha$, Cu $K\alpha$, Hg $L\alpha$ and Pb $L\alpha$ fluorescence lines are 61, 4356, 8209, 302 and 13,905, respectively) **f** Analysis location 22 (the intensity maxima of the Ca $K\alpha$, Fe $K\alpha$, Cu $K\alpha$, Hg $L\alpha$ and Pb $L\alpha$ fluorescence lines are 44, 1550, 496, 129 and 11,625, respectively)

is high, the crescent moons could not be clearly identified. By means of CXRF scans at depth-scan locations 11–17, the first and second coat of arms showed a clear separation between the different layers. This separation was also proven to be due to a varnish thanks to the observation of the cross section A sampled adjacent to the depth-scan location 11. The third coat of arms could only be analyzed at location 13 as it had already been partially removed.

Cross The profiles for the depths-scans at analysis location 8 and 22 correspond to the cross. The CXRF depth profiling at the analysis location 8 reveals five possible layers (Fig. 6e). At the surface of the painting, a Ca- and Hg-based layer is followed by a Pb-based layer with Fe. This could be attributed to the light beige cross which could be composed of lead white mixed with earth pigments and vermillion. Below these two, a third Cu-based (green copper pigment) layer followed by a Fe-based layer (earth pigments), corresponding to the dark triangle on the floor below the cross. Finally, the fifth layer containing Pb (lead white) and Hg (vermillion) likely corresponds to the beige floor.

In Fig. 6f, the depth profiles at the analysis location 22 are shown. Four layers can be seen. On the surface of the painting, a Hg- and Ca-based layer (red vermillion) with some Cu can be found, followed by a Pb- and Fe-based layer (lead white with earth pigments). This likely corresponds to the cross. More in depth, a Cu-based layer is found, followed by a layer containing Pb. This could be the red cape from the saint. The color of the cape is probably made of red lake, not detectable by XRF analysis, mixed with lead white and a little Cu-based pigment.

The presence of the cross is likely linked to the iconographic change of the donor into the monk. As can be seen in the MA-XRF maps of the Fe, the triangles in the floor are all painted under the cross. It was hypothesized that, when the donor was converted into a monk, the cross could have also been added. After the CXRF depth scans at the locations 4, 8, 9 and 22, corresponding, respectively, to the cross over a triangle, over a dark triangle, over the hand and over the red saint's cape, only a slight separation between the layers was found, unlike in the other two areas of interest. Taking this and the information obtained on the cross section C that no varnish was found between the cross and the dark triangle, allows us to conclude that no or only a very thin varnish layer was placed between the cross and the triangles of the floor. Further art-historical studies are necessary to clarify the moment of the addition of the cross.

4 Conclusions

A combination of MA-XRF and CXRF supported by SEM–EDX cross-sectional analysis allowed the study of the hidden layers in the painting *Virgin and Child surrounded by saints and donor* conserved in the Louvre Museum collections in Paris, France. This study brought insights into its history and supported the decision-making process of its restoration. An in-depth vision of the stratigraphy was previously hampered by the fact that MA-XRF does not offer a depth resolution, and that the sampling required to study cross sections with SEM–EDX is very restricted and has to be reduced as much as possible. The advantage of using CXRF is clear, as it can give spatially resolved results on the painting stratigraphy close to those obtained by SEM–EDX on cross sections but in a noninvasive way, allowing to freely increase the number of analysis points and reduce the sampling needed, making the time the main constraint.

Considering the elemental distributions related to the use of different pigments in several areas and depths, it is possible to discuss the changes in the areas of interest found in the MA-XRF scan. In the monk's tunic and in the coat of arms several successive interventions were separated. In the case of the monk's tunic, a shorter dress was found under the visible one. In the coat of arms, three versions painted one on top of each other were found. The clear separation between the layers forming the monk's tunic and the donor's feet, donor's tunic, and bishop's dress, as well as between the different coat of arms, is due to an organic varnish layer, whose composing light elements cannot be evidenced by CXRF. This layer was confirmed to exist in two cross sections analyzed with SEM–EDX and FTIR.

In the case of the cross, no well-separated layer system was found in contrast to the two other considered areas of the painting, perhaps indicating the absence of varnish between the layers. This could indicate that the cross was added at different time than the other iconographic changes of the painting.

This case study highlights the new noninvasive possibilities provided by MA-XRF scanning in combination with CXRF. These combined methods can be applied to other paintings presenting overpaints or compositional changes. The reproducibility of the analyzed point at the microscale is crucial in this methodological combination for correct data interpretation because of the highly heterogeneous nature of paints.

Supplementary Information The online version contains supplementary material available at <https://doi.org/10.1140/epjp/s13360-022-03596-5>.

Acknowledgements We thank Brice Moignard, Antoine Zink and Frédéric Leblanc from the C2RMF laboratory for their help during the reinstallation of the confocal X-ray fluorescence spectrometer. We also thank Gilles Bastian, Clarisse Delmas, Rosaria Motta, Matthieu Gilles and Sophie Caron for the insight they gave us regarding the painting's history and the discussions regarding its restoration. Funding was provided by ANR DepthPaint (ANR-20-CE29-0018) for the CXRF measurements and the PhD of J.T.R. at PSL University, ED 388 (2021-24).

Author contributions The manuscript was written and edited through contributions of J.T., I.R., M.E., T.C and L.P. E.L. performed the MA-XRF data acquisition. M.E. performed the SEM–EDX and FTIR on cross sections data acquisition. J.T., I.R., M.E., T.C. and L.P. have contributed to the CXRF data acquisition. J. T. treated the CXRF data. E.L. and J.T. treated the MA-XRF data. Data evaluation and interpretation was jointly performed by J.T., M.E. and I.R. All authors have given approval to the final version of the manuscript.

Funding ANR DepthPaint, ANR-20-CE29-0018, Thomas Calligaro and Ina Reiche.

Data Availability Statement All data presented and discussed in this manuscript are either presented in the main manuscript file or in the supplementary information. Further information can be provided on demand by the author's institution.

Declarations

Conflicts of interest There is no conflict of interest to declare.

Open Access This article is licensed under a Creative Commons Attribution 4.0 International License, which permits use, sharing, adaptation, distribution and reproduction in any medium or format, as long as you give appropriate credit to the original author(s) and the source, provide a link to the Creative Commons licence, and indicate if changes were made. The images or other third party material in this article are included in the article's Creative Commons licence, unless indicated otherwise in a credit line to the material. If material is not included in the article's Creative Commons licence and your intended use is not permitted by statutory regulation or exceeds the permitted use, you will need to obtain permission directly from the copyright holder. To view a copy of this licence, visit <http://creativecommons.org/licenses/by/4.0/>.

References

1. T. Trojek, R. Prokeš, R. Šefců, H. Bilavčíková, T. Čechák, Confocal X-ray fluorescence spectrometer for in-situ analyses of paintings. *Radiat. Phys. Chem.* **137**, 238–242 (2017). <https://doi.org/10.1016/j.radphyschem.2016.02.031>
2. E. Ravaut, L. Pichon, E. Laval, V. Gonzalez, M. Eveno, T. Calligaro, Development of a versatile XRF scanner for the elemental imaging of paintworks. *Appl. Phys. A* **122**, 17 (2016). <https://doi.org/10.1007/s00339-015-9522-4>
3. M. Eveno, E. Mysak, K. Müller, G. Bastian, N. Pincas, I. Reiche, Confocal XRF depth profiling non-destructively reveals the original blue pigments in a Renaissance painting by Caroto. *Stud. Conserv.* **61**, 102–112 (2016). <https://doi.org/10.1080/00393630.2016.1142059>

4. M. Alfeld, K. Janssens, Strategies for processing mega-pixel X-ray fluorescence hyperspectral data: a case study on a version of Caravaggio's painting Supper at Emmaus. *J. Anal. At. Spectrom.* **30**(3), 777–789 (2015). <https://doi.org/10.1039/C4JA00387J>
5. M. Eveno, E. Ravaud, T. Calligaro, L. Pichon, E. Laval, The Louvre Crucifix by Giotto—Unveiling the original decoration by 2D-XRF, X-ray radiography, Emission spectroscopy and SEM-EDX analysis. *Herit. Sci.* **2**, Article no. 17 (2014). <https://doi.org/10.1186/s40494-014-0017-y>
6. I. Reiche, K. Müller, E. Mysak, M. Eveno, B. Mottin, Toward a three-dimensional vision of the different compositions and the stratigraphy of the painting *L'Homme blessé* by G. Courbet: coupling SEM-EDX and confocal micro-XRF. *Appl. Phys. A* **121**(3), 903–913 (2015). <https://doi.org/10.1007/s00339-015-9428-1>
7. I. Reiche, K. Müller, M. Eveno, E. Itié, M. Menu, Depth profiling reveals multiple paint layers of Louvre Renaissance paintings using non-invasive compact confocal micro-X-ray fluorescence. *J. Anal. Spectrom.* **27**(10), 1715–1724 (2012). <https://doi.org/10.1039/C2JA30157A>
8. W.M. Gibson, M.A. Kumakhov, Applications of x-ray and neutron capillary optics. in: *Yearbook of Science & Technology*, pp. 488–490. McGraw-Hill, New York (1993)
9. B. Kanngießer, W. Malzer, I. Reiche, A new 3D micro X-ray fluorescence analysis set-up—first archaeometric applications. *Nucl. Instrum. Methods Phys. Res. Sect. B Beam Interact. Mater. At.* **211**(2), 259–264 (2003). [https://doi.org/10.1016/S0168-583X\(03\)01321-1](https://doi.org/10.1016/S0168-583X(03)01321-1)
10. B. Kanngießer, W. Malzer, A.F. Rodriguez, I. Reiche, Three-dimensional micro-XRF investigations of paint layers with a tabletop setup. *Spectrochim. Acta Part B* **60**(1), 41–47 (2005). <https://doi.org/10.1016/j.sab.2004.10.012>
11. B. Kanngießer, W. Malzer, I. Mantouvalou, D. Sokaras, A.G. Karydas, A deep view in cultural heritage—confocal micro X-ray spectroscopy for depth resolved elemental analysis. *Appl. Phys. A* **106**, 325–338 (2012)
12. T. Sun et al., Application of confocal X-ray fluorescence micro-spectroscopy to the investigation of paint layers. *Appl. Radiat. Isot.* **94**, 109–112 (2014). <https://doi.org/10.1016/j.apradiso.2014.07.019>
13. K. Nakano, K. Tsuji, Development of laboratory confocal 3D-XRF spectrometer and nondestructive depth profiling. *J. Anal. At. Spectrom.* **25**(4), 562 (2010). <https://doi.org/10.1039/B916974A>
14. I. Mantouvalou et al., A compact 3D micro X-ray fluorescence spectrometer with X-ray tube excitation for archaeometric applications. *J. Anal. At. Spectrom.* **25**(4), 554 (2010). <https://doi.org/10.1039/B915912F>
15. P. Wrobel et al., LabVIEW control software for scanning micro-beam X-ray fluorescence spectrometer. *Talanta* **93**, 186–192 (2012). <https://doi.org/10.1016/j.talanta.2012.02.010>
16. B. Patterson, G. Havrilla, Three-dimensional elemental imaging using a confocal X-ray fluorescence microscope. *Am. Lab.* **38**, 15–22 (2006)
17. S. Smolek, B. Pemmer, M. Fölser, C. Strelci, P. Wobruschek, Confocal micro-x-ray fluorescence spectrometer for light element analysis. *Rev. Sci. Instrum.* **83**(8), 083703 (2012). <https://doi.org/10.1063/1.4744934>
18. A. Markowicz, D. Węgrzynek, S. Bamford, E. China-Cano, Activities in the IAEA X-ray fluorescence laboratory at Seibersdorf. *X-Ray Spectrom.* **35**(4), 207–214 (2006). <https://doi.org/10.1002/xrs.897>
19. K. Müller, M. Eveno, E. Mysak, M. Menu, I. Reiche, Non-invasive depth profiling of paint layers on easel paintings by means of confocal micro x-ray fluorescence versus classical analytical methods, in *ICOM-CC 17th Triennial Conference Preprints*, Melbourne, 15–19 September 2014, ed. J. Bridgland, art. 1607, 8 pp. Paris: International Council of Museums (ISBN 978-92-9012-410-8)
20. K. Müller, B. Hartwig, S. Stelzig, I. Reiche, An in situ non-invasive study of paint layers on Early Netherlandish paintings: new insights into the paintings' history by portable CXRF, in *ICOM-CC 18th Triennial Conference Preprints*, Copenhagen, 4–8 September 2017, ed. J. Bridgland, p. 1607. Paris: International Council of Museums
21. I. Reiche et al., New insights into the painting stratigraphy of *L'Homme blessé* by Gustave Courbet combining scanning macro-XRF and confocal micro-XRF. *Appl. Phys. A* **122**(11), 947 (2016). <https://doi.org/10.1007/s00339-016-0457-1>
22. V.A. Solé, E. Papillon, M. Cotte, P. Walter, J. Susini, A multiplatform code for the analysis of energy-dispersive X-ray fluorescence spectra. *Spectrochim. Acta Part B At. Spectrosc.* **62**, 63–68 (2007)